

# Detection and Localization of Prostate Carcinoma and Benign Prostatic Hyperplasia using DTI

J. Xu<sup>1</sup>, P. Humphrey<sup>2</sup>, A. Kibel<sup>3</sup>, S-K. Song<sup>1,4</sup>

<sup>1</sup>Department of Chemistry, Washington University in St. Louis, St. Louis, Missouri, United States, <sup>2</sup>Department of Pathology & Immunology, Washington University School of Medicine, St. Louis, Missouri, United States, <sup>3</sup>Department of Surgery, Washington University School of Medicine, St. Louis, Missouri, United States, <sup>4</sup>Department of Radiology, Washington University School of Medicine, St. Louis, Missouri, United States

## Introduction

Despite its widespread use in prostate cancer management, conventional MRI has not proven specific enough to guide localized treatment. Recently, significantly improved prostate-to-cancer contrast was achieved using diffusion weighted imaging (DWI) in a transgenic mouse model of spontaneous prostate cancer in vivo (1). To examine the potential of this imaging modality in human prostate, nine radical prostatectomy specimens were examined using diffusion tensor imaging (DTI) with histological correlation.

## Material and methods

### MRI

Human prostate specimens were fixed in formalin for more than 24 hrs before DTI scans. A multislice spin-echo imaging sequence, modified by adding the Stejskal-Tanner diffusion sensitizing gradient pair, was employed for acquisition of the required DWI data set. The diffusion weighted images were acquired with repetition period (TR) 3 s, spin echo time (TE) 35 ms, time between application of gradient pulses ( $\Delta$ ) 12ms, diffusion gradient on time ( $\delta$ ) 4ms, slice thickness (thk) 0.5 mm, field of view (FOV)  $6.5 \times 6.5$  cm, data matrix  $128 \times 128$ , yielding a final resolution of  $0.5\text{mm}^3$ . Diffusion sensitizing gradients were applied along six directions:  $[G_x, G_y, G_z] = [1,1,0], [1,0,1], [0,1,1], [-1,1,0], [0,-1,1],$  and  $[1,0,-1]$ . Two diffusion sensitizing factors or  $b$  values = 0.014 and  $1.361 \text{ ms}/\mu\text{m}^2$  were used to calculate ADC.

### Histology

All specimens were step-sectioned at 4 mm intervals. Individual sections were carefully labeled to permit localization of each section within the prostate. After paraffin embedding, all slides were stained with hematoxylin and eosin. Slides were examined and color-coded for the carcinoma and benign prostatic hyperplasia (BPH) with black and red, respectively.

## Results and Discussions

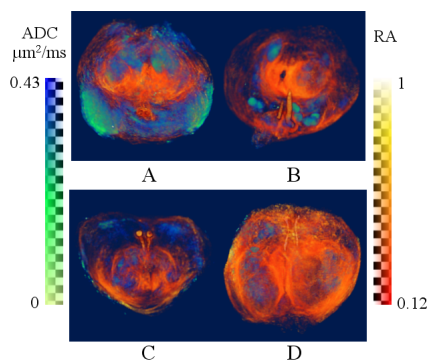


Fig.1 3D reconstructed ADC and RA maps with different histologically-defined extents of carcinoma: A 40%, B 16%, C <5%, D 1%.

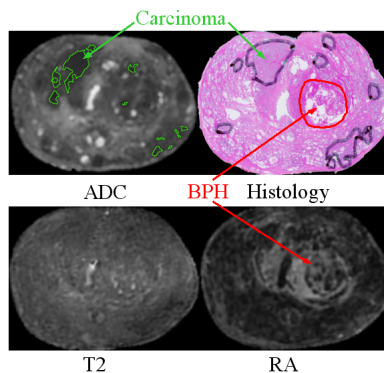


Fig.2 Matching histology with MRI in 2D slices for specimen B. in Fig.1.

Histology	MRI
40%	26%
26%	18%
16%	7%
8%	3%
<5%	3%
4%	4%
4%	3%
1%	2%
1%	2%

Table.1 Correlation of extent of carcinoma for nine different specimens.

Fig. 1 shows the 3D reconstructed maps overlaying ADC and RA. Individual maps were imported into blue-green and yellow-orange channels, respectively. The 3D visualization algorithm, incorporating the 3D connectivity and volume density information, offers significant advantage over 2D maps. Carcinoma is identified on the ADC channel (blue-green) with ADC threshold of  $0.43 \mu\text{m}^2/\text{ms}$  as bright green regions. Bilateral extracapsular extension of the carcinoma was identified in the large tumor specimens in Fig. 1A and was later verified by histology. BPH has a distinct feature in RA map as shown in Fig. 1D. The bright baggy structure delineates the BPH resulting from the high anisotropy in the fibrous connective-tissue capsule of the benign tumor.

Segmentation of carcinoma in the 2D slices for MR and histology comparisons were guided by the use of 3D images as shown in Fig.1. The result for the specimen in Fig. 1B is displayed and compared with histology in Fig 2. Matching of histology and MRI slices was achieved based on the intra-prostate anatomy such as the shape and orientation of the urethra and ejaculator ducts. A perfect match is not easily achieved due to slice misalignment and tissue deformation in the histological mounting and cutting process. Estimation of the extent of carcinoma is better predicted using ADC than T2 map.

The extent of carcinoma estimated from MRI data (reported as percent of prostate gland involved by carcinoma) is shown in Table 1 and compared with the histological determined extent of tumor, which was estimated by a grid morphometric method (2). Discrepancy between MRI and histology estimation exists especially in the specimens with large carcinoma.

## Conclusions

In ex vivo human prostate specimens, carcinoma exhibits a significantly decreased ADC value. Carcinoma and BPH can be identified in 3D reconstructed ADC and RA maps, respectively. Both the size and the location of the histological defined lesions correlate well with those identified by MRI.

## Reference

1. Song, et al *Cancer Res* 62: 1555-1558 (2002)
2. Humphrey, et al *Hum Pathol* 21: 799-804 (1990)